Hybrid-Field Channel Estimation for Extremely Large-Scale Massive MIMO System

Zhentao Hu *Member, IEEE*, Chaoyu Chen, Yong Jin *Member, IEEE*, Lin Zhou *Member, IEEE*, Qian Wei *Member, IEEE*

***Abstract*—Hybrid-field channel estimation for extremely large-scale massive MIMO (XL-MIMO) system is discussed in this paper. By exploiting the structural characteristics of far-field path components in the angle domain and the sparsity of near-field path components in the polar domain, a channel estimation algorithm combining support detection and orthogonal matching pursuit (SD-OMP) is proposed. Specifically, the supports of the far-field path components are firstly detected according to components structure characteristics of the angle domain in the XL-MIMO system and then can be used to obtain the far-field path components. Next, effect on the XL-MIMO system induced by far-field path components can be removed firstly and the OMP algorithm is employed to obtain the near-field path components by exploiting its polar domain sparsity. Finally, the hybrid-field channel is recovered by superposing the given far-field path components and near-field path components. Experiment results show that the proposed algorithm can accurately recover channel with relatively low pilot overhead and computation complexity comparing with some classical channel estimation algorithms.**

***Index Terms*—Hybrid-field, channel estimation, XL-MIMO, pilot overhead.**

I. Introduction

THE 6G communication system on ultra-high frequency band can integrate an extremely large-scale massive MIMO ((XL-MIMO) antenna array in a limited space, thus it can employ beamformer to form a narrower directional beam to compensate the path loss, resulting in service quality of mobile terminals enhancing [1]. As is known to all, using XL-MIMO antenna array will lead to high power consumption, hybrid precoding technology which can reduce antenna transmitters of radio-frequency (RF) chain is considered to be a suitable strategy to handle above problem [2]. However, reducing RF chain will lead hard synchronization of each antenna which reduces accuracy of channel estimation. Although some methods were proposed to enhance the accuracy of channel estimation by lengthening pilot, those methods suffer the poor communication efficiency.

Exploiting sparsity of channel to accurately obtain the channel state information (CSI) may be a suitable scheme with high communication efficiency. For example, Carvalho et al. employed the low rank property of the channel and the angle-domain information to recover the far-field channel [3]. Supposing the channel coefficient following the Gaussian-Bernoulli distribution, Vlachos et al. employed message passing (MP) algorithm to estimate angle-domain sparse channel [4]. Lee et al. used compressive sensing (CS) method to estimate the channel with low pilot overhead [5]. By mapping channel from the array space into the beam space, Gao et al. proposed support detection (SD) algorithm to accurately estimate channel with limited pilot length [6]. It is clear that above researches all focus on far-field planar wave channel, thus are hardly to be directly extended to the near-field spherical wave channel scene. Han et al. divided the large antenna array into multiple sub-arrays firstly and then employed OMP algorithm on sub-arrays to estimate near-field channel [7]. By utilizing polar-domain sparsity of near-field channel, Cui et al. employed on-grid simultaneous orthogonal matching pursuit (SOMP) to efficiently estimate near-field channel firstly and then proposed off-grid simultaneous iterative gridless weighting (SIGW) algorithms to enhance the accuracy of SOMP algorithm [8].

It's worth noting that the above works are suitable for the far-field channel or near-field channel alone, thus they are hard to extend to the scene of XL-MIMO hybrid-field channel which is superimposed by the far-field channel and near-field channel. Very recently, according to angle-domain sparsity of the far-field path components and the polar-domain sparsity of the near-field path components, Wei et al. employed OMP algorithm to successively estimate far-field path components and near-field path components of hybrid-field channel. Since it is not to deeply exploit the structure of the far-field path components, Wei's method is hard to obtain the accurate CSI of the high-dimension hybrid-field channel by using low pilot overhead [9].

By exploiting the structure characteristics of far-field path components in the angle domain and the sparsity of near-field path components in the polar domain, we combine support detection algorithm and orthogonal matching pursuit algorithm to propose a hybrid-field channel estimation algorithm (SD-OMP) here. Specifically, the supports of angle-domain components related to far-field path are obtained by successively employing space structure characteristics of angle-domain components firstly. And then, the effect on receiver induced by far-field path components can be removed, and the near-field path components are obtained by sequentially using OMP algorithm. Finally, the hybrid-field channel is recovered by

This work was supported in part by the National Science Foundation Council of China (61976080), in part the Key Research Projects of University in Henan Province, China (21A413002), in part the Programs for Science and Technology Development of Henan Province, China (212102310298, 222102210002, 222102210088), in part by the Innovation and Quality Improvement Program Project for Graduate Education of Henan University (SYL20060143, SYLKC2022013), in part the Academic Degrees Graduate Education Reform Project of Henan Province (2021SJGLX195Y)

Zhentao Hu, Chaoyu Chen, Yong Jin, Lin Zhou and Qian Wei are with School of Artificial Intelligence, Henan University, Zhengzhou, 450046, China. Chaoyu Chen is the corresponding author (e-mail: 995911928@qq.com).

superposing the given far-field path components and near-field path components. Simulation results show that comparing with the comparison algorithms, the proposed algorithm can achieve more accurate channel estimation with lower pilot overhead and computation complexity.

The rest of this paper is organized as follows. In section II, the XL-MIMO communication system model is introduced. In section III, the SD-OMP algorithm suitable for hybrid-field channel estimation is proposed. The simulation results are provided in section IV, and the conclusion is shown in section V.

Notation: light symbols, boldface lower-case symbols and upper-case symbols denote scalars, vectors and matrices, respectively. $(\cdot)^H$ and $(\cdot)^\dagger$ denote the conjugate transpose, pseudo-inverse respectively. $|\cdot|$ and $\|\cdot\|_2$ denote the absolute operator and the l_2-norm, respectively. $\mathrm{Card}\,(\cdot)$ denotes the cardinality of set.

II. System Model

A XL-MIMO hybrid-field communication system working on time division duplexing (TDD) mode is shown in the Fig. 1, where the BS is equipped with extremely large-scale antenna array to serve a user with single-antenna. The hybrid-field channel from the BS to the user $\mathbf{h} \in \mathbb{C}^{L\times 1}$ is superposed by the far-field path components $\mathbf{h}_F \in \mathbb{C}^{L\times 1}(d > D)$ and the near-field path components $\mathbf{h}_N \in \mathbb{C}^{L\times 1}(d < D)$, where d is the distance from the BS to the scatter, R is the aperture of array antenna, λ is the wavelength and $D = 2R^2/\lambda$ is the Rayleigh distance.

On the one hand, the far-field path components $\mathbf{h}_F$ can be expressed as

$$\mathbf{h}_F = \sqrt{\frac{L}{K}} \sum_{k_f=1}^{K_F} \beta_{k_f} \mathbf{a}\left(\phi_{k_f}\right), \tag{1}$$

where K and K_F represent the number of hybrid-field channel components and the number of far-field path components, respectively. β_{k_f} and ϕ_{k_f} respectively represent the complex gain and the azimuth angle of the k_f-th far-field path component. $\mathbf{a}\left(\phi_{k_f}\right) \in \mathbb{C}^{L\times 1}$ described in the (2) is the far-field array steering vector

$$\mathbf{a}\left(\phi_{k_f}\right) = \frac{1}{\sqrt{L}}\left[1, e^{-j2\pi\phi_{k_f}}, \cdots, e^{-j2\pi(L-1)\phi_{k_f}}\right]^H. \tag{2}$$

where $\phi_{k_f} = \frac{\rho}{\lambda}\cos(\psi)$, ψ is physical angle, and $\rho = \lambda/2$ is the spacing between antennas.

Since the BS is usually placed in high position with limited scatterers, the far-field path components show the sparsity in the angle domain. Thus, in the (3), the far-field path components $\mathbf{h}_F$ can be described by the product of sparse angle-domain path components $\mathbf{h}_f$ and the discrete fourier transform (DFT) matrix $\mathbf{U} = [\mathbf{a}\left(\bar{\phi}_1\right), \mathbf{a}\left(\bar{\phi}_2\right), \cdots, \mathbf{a}\left(\bar{\phi}_L\right)]^H$

$$\mathbf{h}_F = \mathbf{U}\mathbf{h}_f, \tag{3}$$

where $\bar{\phi}_l = \frac{1}{L}(l - \frac{L+1}{2})$ with $l = 1, 2, \cdots L$, represents the pre-defined spatial direction of the XL-MIMO system.

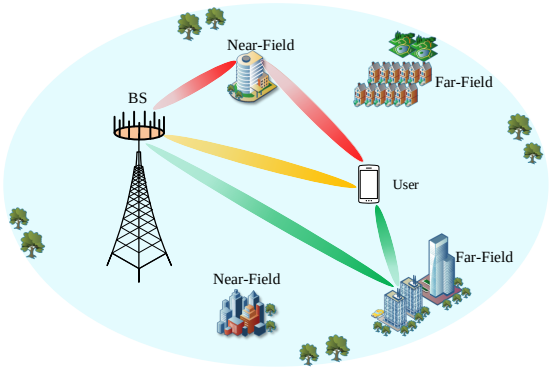

Fig. 1. The hybrid-field communication system for XL-MIMO.

On the other hand, the near-field path components $\mathbf{h}_N$ can be expressed as

$$\mathbf{h}_N = \sqrt{\frac{L}{K}} \sum_{k_n=1}^{K_N} \eta_{k_n} \mathbf{b}\left(\phi_{k_n}, d_{k_n}\right), \tag{4}$$

where K_N, η_{k_n}, ϕ_{k_n} and d_{k_n} represent the number of near-field path components, the complex gain, the azimuth angle and the distance of the k_n-th near-field path component, respectively. $\mathbf{b}\left(\phi_{k_n}, d_{k_n}\right) \in \mathbb{C}^{L\times 1}$ is the near-field array guidance vector [8], which can be denoted by

$$\mathbf{b}\left(\phi_{k_n}, d_{k_n}\right) = \frac{1}{\sqrt{L}}\left[e^{-j\frac{2\pi}{\lambda}\left(d_{k_n}{}^{(1)} - d_{k_n}\right)}, \cdots, e^{-j\frac{2\pi}{\lambda}\left(d_{k_n}{}^{(L)} - d_{k_n}\right)}\right]^H. \tag{5}$$

where $d_{k_n}^{(l)} = \sqrt{d_{k_n}^2 - 2d_{k_n}\omega\rho\phi_{k_n} + \omega^2\rho^2}$ is the distance between the scatterer k_n and the l-th antenna of the BS, $\omega = \frac{2l-L-1}{2}$.

As the near-field path components in the polar domain are sparse too [8], the polar domain transformation matrix related to the array steering vector of the near-field path components can be denoted by

$$\mathbf{V} = \left[\mathbf{b}\left(\phi_1, d_1^1\right), \cdots, \mathbf{b}\left(\phi_1, d_1^{Q_1}\right), \cdots, \mathbf{b}\left(\phi_L, d_L^1\right), \cdots, \mathbf{b}\left(\phi_L, d_L^{Q_L}\right)\right], \tag{6}$$

where ϕ_l and $d_l^{q_l}$ $(q_l = 1, 2, \cdots, Q_l)$ represent the sampled azimuth angle and distance between the scatterer and the BS at the l-th antenna, respectively. Q_l is the number of sampled distances at azimuth angle ϕ_l, thus the number of sampled distances at all antennas can be denoted by $Q = \sum_{l=1}^{L} Q_l$.

Similar to the far-field path components, the near-field path components $\mathbf{h}_N$ can be described as the product of the polar-domain transform matrix $\mathbf{V}$ and the polar-domain sparse path components $\mathbf{h}_n$.

$$\mathbf{h}_N = \mathbf{V}\mathbf{h}_n, \tag{7}$$

Thus, by superposing the far-field path components and the near-field path components, the channel in the hybrid-field can be expressed as

$$\mathbf{h} = \sqrt{\frac{L}{K}} \left(\sum_{k_f=1}^{\alpha K} \beta_{k_f} \mathbf{a}\left(\phi_{k_f}\right) + \sum_{k_n=1}^{(1-\alpha)K} \eta_{k_n} \mathbf{b}\left(\phi_{k_n}, d_{k_n}\right) \right), \tag{8}$$

where $\alpha K = K_F$ and $(1-\alpha)K = K_N$ respectively represent the number of far-field path components and near-field path components in the hybrid-field channel, and $\alpha \in [0,1]$ is the control variable.

Furthermore, the hybrid-field channel can be expressed by superimposing of (3) and (7)

$$\mathbf{h} = \mathbf{U}\mathbf{h}_f + \mathbf{V}\mathbf{h}_n, \tag{9}$$

To estimate the hybrid-field channel, the user should send the given orthogonal pilot signal to the BS in the time slots with length W. The pilot signal received by the BS can be expressed by

$$\mathbf{y} = \mathbf{G}\mathbf{h} + \mathbf{x}, \tag{10}$$

where the matrix $\mathbf{G} \in \mathbb{C}^{L\times 1}$ represents the orthogonal pilot sequence that the user sends to the BS in the W time slots, and $\mathbf{x} \sim \mathcal{CN}\left(0, \mu^2 \mathrm{I}_W\right)$ is the noise of the BS.

III. Proposed Channel Estimation Algorithm

A. SD-OMP Algorithm

Substituting the (9) into the (10), the received pilot signal can be equivalently represented as

$$\mathbf{y} = \mathbf{G}\mathbf{U}\mathbf{h}_f + \mathbf{G}\mathbf{V}\mathbf{h}_n + \mathbf{x}, \tag{11}$$

where the far-field sparse path components in the angle domain can be expressed as $\mathbf{h}_f = \mathbf{U}^H\mathbf{h}_F = \sqrt{\frac{L}{K}} \sum_{k_f=1}^{K_F} \mathbf{U}^H \beta_{k_f} \mathbf{a}\left(\phi_{k_f}\right)$ in which the k_f-th component $\mathbf{z}_{k_f} = \mathbf{U}^H \beta_{k_f} \mathbf{a}\left(\phi_{k_f}\right)$ is approximately orthogonal with the other components due to the large number of BS antennas. Therefore, $\mathbf{h}_f$ can be obtained by sequentially estimating its each component. Specifically, we can firstly estimate the strongest component of $\mathbf{h}_f$, and then erase its influence on receiver to estimate the second strongest component of $\mathbf{h}_f$ until all the components of $\mathbf{h}_f$ is obtained.

The details of how to determine components of $\mathbf{h}_f$ are described as follows. Firstly, current research shows that ratio between total energy of the one far-field component and M strongest energy elements of this component satisfies the following inequality [6].

$$\frac{p_M}{p_Z} \geq \frac{2}{L^2} \sum_{\tau=1}^{M/2} \frac{1}{\sin^2\left(\frac{(2\tau-1)\pi}{2L}\right)}, \tag{12}$$

where p_Z is the total energy of component and p_M is the energy of M strongest energy elements in this component. L is the dimension of component. We can find the (12) indicates that the total energy of the one component is only determined by few of elements in this component. Moreover, [6] also demonstrates that this few of elements must uniformly revolve around the strongest energy element. Thus, as described in the (13), M strongest energy elements can form the support of component $\mathbf{z}_{k_f}$, in which l^* means the position of strongest energy element which can be obtained by maximizing relevance between the sensing matrix and the output of the receiver.

$$\mathrm{Supp}(\mathbf{z}_{k_f}) = \mathrm{mod}_L \left\{ l^* - \frac{M}{2}, \cdots, l^* - 1 + \frac{M}{2} \right\}, \tag{13}$$

where mod_L is the modulo operation with respect to L. By this way, the components of far-field spare path $\mathbf{h}_f$ in the angle domain can be sequentially estimated firstly, thus far-field path components $\mathbf{h}_F$ can be recovered by using the (7). Next, the effect on receiver induced by $\mathbf{h}_F$ can be erased and the near-field path components $\mathbf{h}_N$ can be rebuilt by employing OMP algorithm. The hybrid-field channel is obtained by superposing the far-field path components and near-field path components finally.

The steps of the proposed hybrid-channel estimation called SD-OMP are shown in **Algorithm 1**. We can find this algorithm is composed by three stages. In the first stage, the position of the strongest energy l^* in $\bar{\mathbf{z}}_{k_f}$ is determined by maximizing the correlation between $\mathbf{S}_F$ and $\mathbf{c}$ firstly. Then, support of component $\bar{\mathbf{z}}_{k_f}$ related to far-field path in the angle domain, namely $\mathrm{supp}(\bar{\mathbf{z}}_{k_f})$ is obtained by using (12). Thus, effect on receiver induced by component $\bar{\mathbf{z}}_{k_f}$ can be erased in the step 5. By successively running step 1 to step 8, the supports of K_F components are obtained and the estimation of far-field path components $\bar{\mathbf{h}}_f$ in the

Algorithm 1 SD-OMP Based Hybrid-field Channel Estimation

Inputs: $\mathbf{y}, \mathbf{G}, \mathbf{U}, \mathbf{V}, K_F, K_N, L, Q, M$.

Initialization: $\mathbf{c} = \mathbf{y}, \mathbf{S}_F = \mathbf{G}\mathbf{U}, \mathbf{S}_N = \mathbf{G}\mathbf{V}$.

// Far-field path components in the angle domain estimation stage.

1. **for** $0 \leq k_f \leq K_F$
2. Detect the position of the strongest elment of $\bar{\mathbf{z}}_{k_f}$ as $l^* = \underset{1\leq l\leq L}{\mathrm{argmax}} |\mathbf{S}_F\mathbf{c}|$;
3. $\mathrm{Supp}(\bar{\mathbf{z}}_{k_f}) = \mathrm{mod}_L \left\{ l^* - \frac{M}{2}, \cdots, l^* + \frac{M}{2} \right\}$;
4. $\bar{\mathbf{z}}_{k_f} = \mathbf{0}_{\mathrm{L}\times 1}$, $\bar{\mathbf{z}}_{k_f} = \mathbf{S}_F(:, \mathrm{Supp}(\bar{\mathbf{z}}_{k_f})^\dagger \mathbf{c}$;
5. $\mathbf{c} = \mathbf{y} - \mathbf{S}_F \bar{\mathbf{z}}_{k_f}$;
6. **end**
7. $\mathrm{Supp1} = \underset{0\leq k_f\leq K_F}{\cup} \mathrm{supp}(\bar{\mathbf{z}}_{k_f})$;
8. $\bar{\mathbf{h}}_f = \mathbf{0}_{\mathrm{L}\times 1}, \bar{\mathbf{h}}_f = \mathbf{S}_F(:, \mathrm{Supp1})^\dagger \mathbf{y}$;

// Near-field path components in the polar domain estimation stage.

9. **for** $0 \leq k_n \leq K_N$
10. **for** $0 \leq m \leq \mathrm{M}$
11. $l^* = \underset{1\leq l\leq Q}{\mathrm{argmax}} \|\mathbf{S}_N\mathbf{c}\|_2^2$;
12. $\mathrm{Supp2} = \underset{0\leq m\leq M}{\cup} l^*$;
13. $\bar{\mathbf{h}}_n = \mathbf{0}_{Q\times 1}, \bar{\mathbf{h}}_n = \mathbf{S}_N^\dagger(:, \mathrm{Supp2})\mathbf{y}$;
14. $\mathbf{c} = \mathbf{y} - \mathbf{S}_F\bar{\mathbf{h}}_f - \mathbf{S}_N\bar{\mathbf{h}}_n$;
15. **end**
16. **end**

// Hybrid-field channel estimation stage.

17. $\bar{\mathbf{h}} = \mathbf{0}_{L\times 1}$, $\bar{\mathbf{h}}_F = \mathbf{U}\bar{\mathbf{h}}_f, \bar{\mathbf{h}}_N = \mathbf{V}\bar{\mathbf{h}}_n, \bar{\mathbf{h}} = \bar{\mathbf{h}}_F + \bar{\mathbf{h}}_N$;
18. **end**

Output: Estimated channel $\bar{\mathbf{h}}$.

TABLE I
COMPLEXITY COMPARISON OF DIFFERENT LOCALIZATION ALGORITHMS

Algorithm	Complexity
Hybrid-field SD-OMP	$\mathcal{O}\left(LWK_FM^2\right) + \mathcal{O}\left(W\text{Card}^2(\text{Supp1})\right) + \mathcal{O}\left(QW(K_NM)^3\right) + \mathcal{O}\left(LQ\right)$
Hybrid-field OMP	$\mathcal{O}\left(LW(K_FM)^3\right) + \mathcal{O}\left(QW(K_NM)^3\right) + \mathcal{O}\left(LQ\right)$
Far-field OMP	$\mathcal{O}\left(LW(KM)^3\right) + \mathcal{O}\left(L^2\right)$
Near-field OMP	$\mathcal{O}\left(QW(KM)^3\right) + \mathcal{O}\left(LQ\right)$
MMSE	$\mathcal{O}(WL^2) + \mathcal{O}(L^3)$

TABLE II
SIMULATION PARAMETERS

Parameter	Notations	Value
L	Number of BS antennas	512
f_c	Carrier frequency	30GHz
β	Far-field path gain	$\mathcal{CN}(0,1)$
η	Near-field path gain	$\mathcal{CN}(0,1)$
ψ	Angle distribution	$\mathcal{U}(0,\pi)$
ϕ	Angle distribution	$\mathcal{U}(-1,1)$
d_N	Near-field sampled distance	$\mathcal{U}(10m,100m)$
Q	Number of sampled grids	2071
M	Number of component elements	8

angle domain is achieved too. In the second stage, OMP algorithm is used to obtain the estimation the k_n-th near-field component $\bar{\mathbf{h}}_n$ firstly, and then effect on receiver induced by $\bar{\mathbf{h}}_n$ is eliminated by using the step 14 of **Algorithm 1**. Thus, By repeatedly running step 9 to step 16, the K_N components estimation of near-field path in the polar domain are achieved by maximizing the correlation between the sensing matrix $\mathbf{S}_N$ and $\mathbf{c}$. In the third stage, the far-field path components $\bar{\mathbf{h}}_F$ and the near-field path components $\bar{\mathbf{h}}_N$ are obtained by using $\bar{\mathbf{h}}_F = \mathbf{U}\bar{\mathbf{h}}_f$ and $\bar{\mathbf{h}}_N = \mathbf{V}\bar{\mathbf{h}}_n$, respectively. Finally, $\bar{\mathbf{h}}_F$ and $\bar{\mathbf{h}}_N$ are superimposed to obtain the estimation $\bar{\mathbf{h}}$ of the hybrid-field channel.

B. Complexity Analysis

The computational complexity of the proposed SD-OMP algorithm is shown in Table I. We can find that the computational complexity of the first stage is described as $\mathcal{O}\left(LWK_FM^2\right)+\mathcal{O}\left(W\text{Card}^2(\text{Supp1})\right)$ [6]. Since $\text{Card}(\text{Supp1})$ follows the inequality $\text{Card}(\text{Supp1}) \leq K_FM$ [6], which indicates the computational complexity of the far-field path components estimation related to proposed hybrid-field SD-OMP algorithm is mainly determined by the $\mathcal{O}\left(LWK_FM^2\right)$. The computational complexity of second stage is described as $\mathcal{O}\left(LW(K_NM)^3\right)$ [9]. And the computational complexity of the thrid stage is described as $\mathcal{O}\left(LQ\right)$, thus the total computational complexity of the proposed SD-OMP algorithm is $\mathcal{O}\left(LWK_FM^2\right)+\mathcal{O}\left(W\text{Card}^2(\text{Supp1})\right)+\mathcal{O}\left(LW(K_NM)^3\right)+\mathcal{O}\left(LQ\right)$. In addition, the main the difference of computational complexity between the hybrid-field SD-OMP algorithm and the hybrid-field OMP algorithm [9] lies in the stage of far-field path components estimation. Since the computational complexity of hybrid-field OMP algorithm related to the estimating far-field path components is described as $\mathcal{O}\left(LW(K_FM)^3\right)$ and the $\mathcal{O}\left(LWK_FM^2\right) < \mathcal{O}\left(LW(K_FM)^3\right)$ is always hold on obviously, which means the computational complexity of the proposed SD-OMP algorithm is lower than that of the hybrid-field OMP algorithm.

IV. SIMULATION RESULTS

Experiments comparing with some algorithms including the hybrid-field OMP [9], far-field OMP [5], near-field OMP [8], LS and the minimum mean square error (MMSE) [10] are designed to evaluate the performance of the proposed algorithm in this section. In addition, Genie-aided-LS algorithm which the prior information related to the channel such as the distances and angles between the receivers and scatters [8] are perfectly known is employed as the lower bound of the performance algorithm. A XL-MIMO hybrid-field communication system is described in fig. 1, and the experiments parameters are listed in Table II. The performance of algorithms is evaluated by the normalized mean square error (NMSE) which is defined as $\text{NMSE} \triangleq \left\|\mathbf{h}-\bar{\mathbf{h}}\right\|_2^2 / \left\|\mathbf{h}\right\|_2^2$.

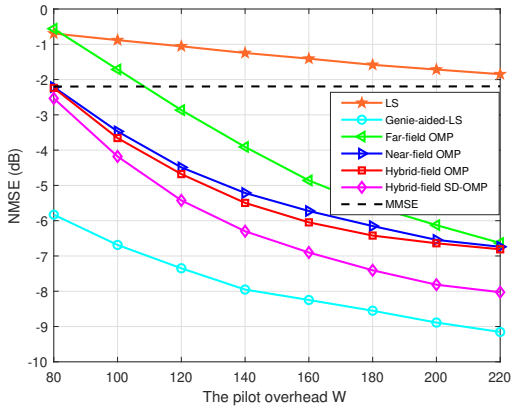

Fig. 2. NMSE versus the pilot overhead W.

The NMSE versus pilot overhead W of algorithms is plotted in Fig. 2, where the SNR, control variable α and channel components K are set as 6dB, 1/3 and 6, respectively. It can be seen that proposed SD-OMP algorithm can achieve the highest accuracy except the Genie-aided-LS in all algorithms. Moreover, the accuracy of the hybrid-field OMP is higher than that of far-field OMP and near-field OMP due to hybrid-field OMP is designed according hybrid-field channel model which is close to experiment scene. In addition, the accuracy of the near-field OMP is higher than that of far-field OMP since the near-field path components are the dominant in the hybrid-field channel. What's more, since employs OMP algorithm instead of SD algorithm to estimate components of far-field path components, hybrid-field OMP suffer lower accuracy of far-field path components than that of hybrid-field SD-OMP, leading to lower estimation accuracy of hybrid-field channel comparing with that of hybrid-field SD-OMP.

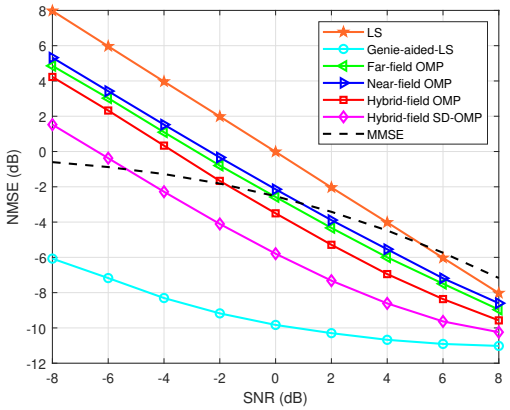

Fig. 3. NMSE versus the SNR .

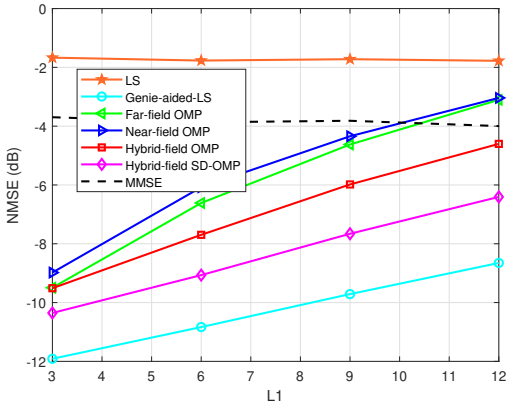

Fig. 4. NMSE versus channel components K.

Besides, since its estimation accuracy is mainly determined by SNR rather than the pilot overhead, the MMSE algorithm experiences roughly same estimation accuracy with number of pilot overhead changing.

Fig. 3 plots the NMSE of algorithms versus the SNR, where the pilot overhead W, control variable α and channel components K are set as 210, 2/3 and 6, respectively. It can be seen that the NMSE of all algorithms are improved with the SNR increasing. Moreover, the accuracy of the hybrid-field SD-OMP algorithm is the best except the Genie-aided-LS algorithm at the same SNR, since it not only is suitable for describing hybrid-field channel scene but also employs SD algorithm to obtain the most accurate estimation of far-field path components related to hybrid-field channel. In addition, as described in Fig. 2, since uses the algorithm suitable for hybrid-field channel, hybrid-field OMP shows the better MMSE than that of far-field OMP and near-field OMP, and the accuracy of the far-field OMP is higher than that of near-field OMP since the far-field path components are the dominant in the hybrid-field channel. However, since hybrid-field OMP employs OMP instead of SD algorithm to determine the far-field path components, the accuracy of hybrid-field OMP is apparently lower than that of hybrid-field SD-OMP.

Fig. 4 plots the NMSE of algorithms versus channel components K, where the pilot overhead W, SNR and control variable α are set as 220, 5dB and 2/3, respectively. We can find that the NMSE of all algorithms except MMSE algorithm and LS algorithm tend to be deteriorating with the channel components increasing. This is because the channel components K increasing mean the estimated channel parameters increasing, resulting in accuracy of channel estimation declining. However, since its estimation accuracy is mainly determined by SNR rather than the number of channel components, the MMSE algorithm experiences roughly same estimation accuracy with number of channel components changing. What's more, the proposed algorithm still achieves the best accuracy except the Genie-aided-LS, which certifies the effectiveness of the proposed algorithm.

V. Conclusion

In this paper, a low pilot overhead algorithm which exploits the structure of far-field path components and sparsity of near-field path components is proposed to estimate hybrid-field channel of XL-MIMO system working on TDD mode. By employing SD algorithm in far-field path components and OMP algorithm in near-field path components, respectively, proposed SD-OMP algorithm can accurately recover the hybrid-field channel with limited pilot overhead. The simulation results demonstrate the effectiveness of the proposed algorithm. In our future work, we will explore the issue of wideband hybrid-field channel estimation in XL-MIMO system.

References

[1] E. D. Carvalho, A. Ali, A. Amiri, M. Angjelichinoski, and R. W. Heath, Jr., "Non-stationarities in extra-large-scale massive MIMO," *IEEE Wireless Communications Letters*, vol. 27, no. 4, pp. 74–80, Aug. 2020.

[2] L. Dai, B. Wang, M. Peng, and S. Chen, "Hybrid precoding-based millimeter-wave massive MIMO-NOMA with simultaneous wireless information and power transfer," *IEEE Journal on Selected Areas in Communications*, vol. 37, no. 1, pp. 131–141, Jan. 2019.

[3] E. Vlachos, G. C. Alexandropoulos and J. Thompson, "Wideband MIMO Channel Estimation for Hybrid Beamforming Millimeter Wave Systems via Random Spatial Sampling," *IEEE Journal of Selected Topics in Signal Processing*, vol. 13, no. 5, pp. 1136-1150, Sept. 2019.

[4] C. Huang, L. Liu, C. Y uen, and S. Sun, "Iterative channel estimation using LSE and sparse message passing for mmWave MIMO systems," *IEEE Transactions on Signal Processing*, vol. 67, no. 1, pp. 245–259, Jan. 2019.

[5] J. Lee, G.-T. Gil, and Y. H. Lee, "Channel estimation via orthogonal matching pursuit for hybrid MIMO systems in millimeter wave communications," *IEEE Transactions on Communications*, vol. 64, no. 6, pp. 2370–2386, Jun. 2016.

[6] X. Gao, L. Dai, S. Han, C. I and X. Wang, "Reliable Beamspace Channel Estimation for Millimeter-Wave Massive MIMO Systems with Lens Antenna Array," *IEEE Transactions on Wireless Communications*, vol. 16, no. 9, pp. 6010-6021, Sept. 2017.

[7] Y. Han, S. Jin, C.-K. Wen, and X. Ma, "Channel estimation for extremely large-scale massive MIMO systems," *IEEE Communications Letters*, vol. 9, no. 5, pp. 633–637, May. 2020.

[8] M. Cui and L. Dai, "Channel Estimation for Extremely Large-Scale MIMO: Far-Field or Near-Field?" *IEEE Transactions on Communications*, vol. 70, no. 4, pp. 2663-2677, April 2022.

[9] X. Wei and L. Dai, "Channel Estimation for Extremely Large-Scale Massive MIMO: Far-Field, Near-Field, or Hybrid-Field?" *IEEE Communications Letters*, vol. 26, no. 1, pp. 177-181, Jan. 2022.

[10] N. Shariati, E. Björnson, M. Bengtsson and M. Debbah, "Low-Complexity Polynomial Channel Estimation in Large-Scale MIMO With Arbitrary Statistics," *IEEE Journal of Selected Topics in Signal Processing*, vol. 8, no. 5, pp. 815-830, Oct. 2014.